AO05: Ash detection and characterisation in IASI data

Candidate number: 249038
Supervisors: Dr. E. Carboni and Dr. R.G. Grainger
Word count: 5480

Abstract

High resolution infrared spectra from the Infrared Atmospheric Sounding Interferometer (IASI) are used to propose a new and improved detection scheme to distinguish volcanic ash from other airborne substances such as water clouds and desert dust. The method approximates three regions of the infrared spectrum between 840 - 1210 cm^{-1} to linear functions and by calculating their ratios and applying some conditions the ash affected pixels are found. A set of these spectra and two times more of other ash spectra, which were found in different eruptions, are then used for correlation with other pixels to find the ash plume.
Based on simulations of a radiative transfer model some of the properties of the plume are extracted including: optical depth, the cloud top height and the effective radius of ash particles.

1 Introduction

Early detection of natural disasters is of a great importance and the ash clouds produced by volcanic eruptions may cause major problems in aviation safety and have an effect on climate change. Ash released in volcanic explosion can drift up to 30 km high, staying in the upper troposphere for many days or weeks (Mastin et al., 2009). Particles with small radii tend to remain in the air for a long time as the bigger ones fall out under gravitational forces within a few hours (Textor et al,. 2005). Some atmospheric processes, like winds and coagulation, can influence the time of stay of particles in the atmosphere. Over the past few years ash particles have caused severe damage to planes' instruments including engines, blades, air filters etc. and induced many disruptions in air traffic (Miller and Casadevall, 2000). Moreover, ash particles may be charged and so disturb radio communication. Although there has never been any accident with casualties, in the 80s two commercial planes lost their engines and were forced to land (Casadevall, 1994). The eruption of Icelandic volcano Eyjafjallajökull in April 2010 has led to huge problems, causing 200 million dollars of losses a day (Wearden, 2010). The increasing number of incidents led to the creation of nine Volcanic Ash Advisory Centers around the world at the beginning of the 1990s. VAACs are responsible for information about existing volcanic ash clouds and for forecasting their movements.
In recent years, observations of volcanic ash plumes from satellites gained much interest as this method gives global coverage and continuity of data. With the introduction of Atmospheric Infrared Sounder (AIRS) in 2002, and the IASI instrument in 2006, which have about 100 times more channels then the previous apparatus, perspectives for new algorithms have arisen. These two instruments give a complete and precise spectrum in a broad region from 3.6 µm to 15.5 µm. Data from the IASI instrument, which resides on METOP satellite and is a high resolution spectrometer with an instantaneous field of view 12 x 12 km^2 at nadir, were used in this project in the infrared window region from 700 to 1250 cm^{-1} and from 2670 to 2730 cm^{-1} with resolution 0.25 cm^{-1}. These data provide radi-

ance from the Top Of the Atmosphere (TOA) as a function of wavenumber. The radiance is then changed to brightness temperature to better illustrate the spectral signatures of different substances.
The detection of volcanic ash from this kind of instrument can be curtailed, because the volcanic cloud may be overlaid by water or ice cloud. Moreover, water vapour may condense at certain heights and create an icy coat over an ash particle - these are called hydrometeors (Textor et al., 2005). The IR absorption can vary greatly for such particles. In many eruptions some SO_2 is ejected and spectra of ash and SO_2 may interfere.

1.1 Refractive index behaviour for volcanic ash particles

Volcanic ash particles are made up of tephra which are composited of SiO_2, rock and glass and have radii smaller then 2 mm. We can differentiate many types of tephra which have different functions of refractive index with respect to the wavenumber. The imaginary part of the refractive index (n_i) coefficient is responsible for the absorption of the electromagnetic waves in the infrared region. As can be seen in Figure 1, the n_i for materials originating from SiO_2 is generally increasing in the region 800 to 1000-1100 cm^{-1} and decreasing between 1000-1100 and 1250 cm^{-1}. For andesite there is a small dip near 810 cm^{-1} while for rhyolite there is a similar drop but it is further to the right. This shift may be the main reason for the operation of the concavity algorithm written by Gangale et al. (2009) used to flag the rhyolitic ash from the 2008 Chilean eruption (the method is explained further). The imaginary part of the refractive index for hydrous particles is monotonically decreasing for almost the whole spectrum with a peak around 830 cm^{-1} for ice. The absorption behaviour for SiO_2 composites in the 800 to 1000-1100 cm^{-1} region is reverse to that of hydrous particles and this was the basis of the 'split-window' test to detect ash plume written by Fred Prata (1989a, b).

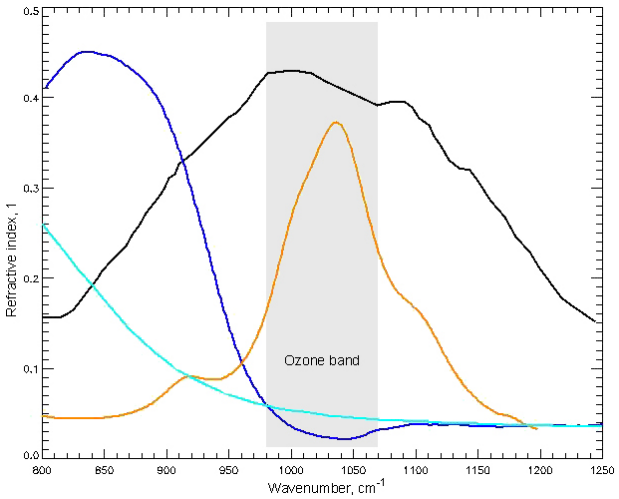

Figure 1: Imaginary part of refrective index as a function of wavenumber for five different materials. Black line represents data for andesite, orange - desert dust, blue - water, dark blue - ice. Data acquired from Aerosol Refractive Index Archive (ARIA), Oxford.

1.2 IASI spectra and ash spectral signatures

In Figure 2 one can see the spectra of andesitic and rhyolitic volcanic ash, water and ice clouds, desert dust and clear scene. As can be noticed, the real spectra have their origin in the refractive index n_i. There is a visible negative slope in the first region for SiO_2 composites and positive for hydrous particles due to absorption features of these aerosols. The flat or almost negative slope in the same region for the clear scene curve is because the radiance is exponentially decreasing with increasing wavenumber, but the optical depth of water vapour (which must be present in the clear scene as well) is growing with respect to wavenumber; hence, the two effects interfere making the spectrum more or less flat. Then there is the ozone band which gives different absorption features and the 1070 - 1210 cm^{-1} region which has positive slope for ash and sand. The specific shape of the spectrum varies with the height of the plume, mineral composition, optical depth, effective size and shape of the particles but in general it is said that it makes up a 'V' shape (Karagulian et al., 2010) between 800 and 1250 cm^{-1}. The spectral properties of the plume change with the age of the cloud as

the bigger particles fall out under gravitational forces.
The slopes in the regions described above have generally opposite monotonicity for water and ice clouds, as is clearly visible in Figure 2.
If a water cloud is present in an area of eruption, or vast amounts of SO_2 were expelled from a volcano, the shape of an ash spectrum may vary remarkably. For example, in the Kasatochi eruption very large amounts of SO_2 were thrown up visibly changing the spectrum in the region 1070 - 1210 cm^{-1}, where the two absorption dips are noticeable (Figure 3). In the initial phase of the Eyjafjallajökull 2010 eruption some ice melted from the top of the mountain creating hydrometeors and affecting the spectrum near 950 cm^{-1} (Clarisse et al., 2010).

1.3 Existing ash detection algorithms

The 'split-window' test (Prata, 1989) was a simple and revolutionary algorithm which could work on data from most of the contemporary instruments. Brightness temperature difference (BTD), which was originally defined in this uncomplicated and fast algorithm as the difference between the brightness temperature of 11 µm and 12 µm, was used in the past 20 years with great success. In AATSR, MODIS, SEVIRI and GOES the two mentioned channels had about 1 µm band width (Figure 2) and calculation of BTD for every pixel gave the discrimination for ash when BTD was negative.

$$BT_{11\mu m} - BT_{12\mu m} < 0$$

For water and ice clouds BTD was generally positive. However, in real situations the 'split-window' test may experience some problems because the ash spectra may interfere with water or ice spectra and cause false detections (Pavalonis et al., 2006). Moreover, there is a noticeable change in BTD range in different eruptions in various atmospheric conditions or climates (Simpson et al., 2000; Prata et al., 2001).
Some tried introducing modifications to the Prata, 1989 method, including the implication of 3.5 µm - 3.9 µm channel which has strong solar

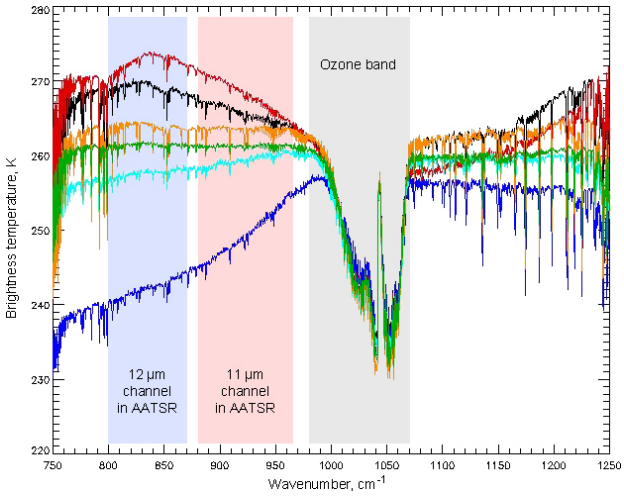

Figure 2: IASI observations of brightness temperature as a function of wavenumber for different pixels containing 5 different scenes. The red line represents data for Chaiten ash 05/05/2008, black - Eyjafjallajökull 07/05/2010, orange - saharan dust 28/04/2010, light blue - water cloud, dark blue - ice cloud, green - clear scene.

and Earth's surface radiation components (Ellrod et al., 2003; Pergola et al., 2004) or incorporating the visible channel data (Mosher, 2000; Pavalonis et al., 2006). However, when using the visible wavelenghts a significant problem may arise because some ash plum may be black, while the others can be brown, grey or even white.
Very low refractive index for ice and water and negative slope for ash in the latter region gave the idea for another ash test which concentrates on this region, but BTD was taken between 1231.5 and 1168 cm^{-1} and must be positive (Clarisse et al., 2010).
Gangale et al. (2009) has made a thorough investigation of the Chaiten eruption in 2008. The volcanic ash in this eruption was rhyolitic (Carn et al., 2009) and had a visible negative concavity in the spectrum. A new algorithm was introduced in this paper which was looking for the quadratic concavity in the region between 800 cm^{-1} and 960 cm^{-1} and some correlation thresholds were also applied.

1.4 The correlation coefficient

Later in the paper the Pearson coefficient will be used: this is a measure of the correlation of two

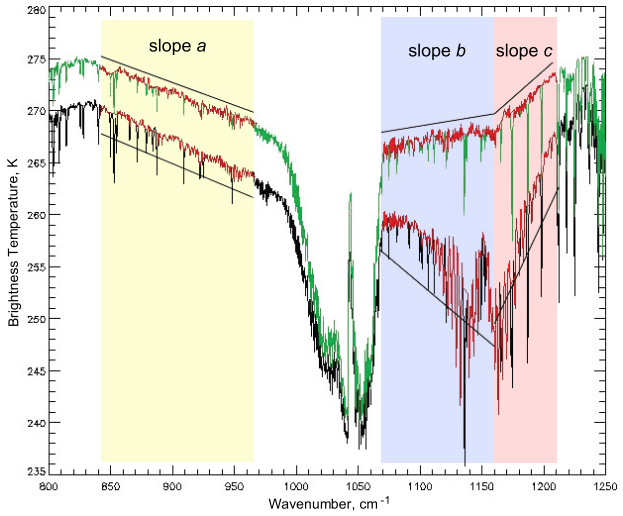

Figure 3: Spectral shapes for two eruptions: green - Eyjafjallajökull eruption 7 May 2010, black - Kasatochi eruption 8 August 2008. The green spectrum is shifted upwards by 5K. Red shows the modified spectra (high absorption H_2O and O_3 bands are excluded) which are used in the tests.

shapes. It is described as a ratio of the covariance between two variables and the multiplication of their standard deviations

$$\rho = \frac{cov(X,Y)}{\sigma_X \sigma_Y}$$

where X and Y are the two samples (in our case these are the two channels of the IASI instrument). In general this equation reads:

$$\rho = \frac{\sum_{i=1}^{n}(X_i - \bar{X})(Y_i - \bar{Y})}{\sqrt{\sum_{i=1}^{n}(X_i - \bar{X})^2}\sqrt{\sum_{i=1}^{n}(Y_i - \bar{Y})^2}}$$

where $\bar{X}$ and $\bar{Y}$ are the sample means. The numerical value of the Pearson correlation coefficient lies between $\rho \in [-1, 1]$ and is equal to 1 if two functions have exactly the same shape, -1 if they are strictly opposite or symmetric and 0 if they are totally unrelated. This mathematical instrument only compares the pattern of the two functions, so that two identical functions which are shifted by a in x-direction and by b in y-direction will still have $\rho = 1$.

A modified correlation coefficient written by Beer and Norton (1987) was also used. It was defined as:

$$H = \frac{\sum_{i=1}^{n}(X_i - \bar{X})^2) - \sum_{i=1}^{n}(Y_i - \bar{Y})^2}{\sum_{i=1}^{n}(X_i - \bar{X})(Y_i - \bar{Y})}$$

However, the application of this device was not very efficient as it was concentrating on absorption similarity of individual peaks visible in Figure 2 or 3, rather than the continuum spectral shape itself.

1.5 Radiative transfer

To retrieve the characteristic properties of the ash plume a simulation based on radiative transfer must be carried out first. The electromagnetic radiation coming to the IASI instrument from below loses energy by absorption, gains energy by emission, additionally this energy is also distributed by scattering processes. Hence, the spectral radiance L_ν which is received by the satellite at given frequency ν may be written as:

$$L_\nu = \int_0^\infty B_\nu(T(z))\frac{\partial \mathcal{T}_\nu(z,\infty)}{\partial z}\mathrm{d}z + B_\nu(T_g)\mathcal{T}_\nu(0,\infty)$$

where B_ν is the black body radiation at temperature $T(z)$ and height z, $\mathcal{T}_\nu$ is the transmittance and T_g is the surface temperature. The simulation must also take into account the scattering of the radiation. The size of the aerosol particles like volcanic ash, desert dust and water vapour droplets is comparable to the wavelength of the electromagnetic radiation coming to the satellite. This kind of scattering is well described by Mie theory if we assume that the particles are spherical, although it is highly probable that they are not.

The Oxford-RAL Retrieval of Aerosol and Cloud (ORAC) assumes inserting a slab of a given substance (e.g. ash, desert dust or water cloud) within an atmosphere. The Mie code is then used with particular optical properties of a given material, as presented in Figure 1, to simulate the scattering mechanisms in the atmosphere.

2 Developing an efficient ash flag

2.1 Method

Initially a 'split-window' test was carried out by averaging the IASI channels with the 11 µm band centred at 924 cm^{-1} and its width 84 cm^{-1} and the 12 µm band was centred at 835 cm^{-1} with width 70 cm^{-1}. These bands correspond to the AATSR 11 and 12 µm channels. The discrimination for the ash was that BTD for these two bands was negative.

$$BT_{924} - BT_{835} < 0$$

This technique was quite a good discriminator for ash in most of the eruptions, but a lot of non-ash pixels, including sand dust, were flagged as well, as can be seen in Figure 5 in columns B and C. The 'split-window' test is working less efficiently when it comes to distinguishing ash from sand storm events because the spectral behaviour of dust and ash particles is very similar in the region 800-980 cm^{-1}.

After analyzing 100s of ash and desert dust curves (which were primarily detected using the stronger conditioned 'split-window' test and MODIS data in the visible region) the conclusion was that these spectra have a negative gradient in the region 800-980 cm^{-1} (slope a) and positive between 1070-1210 cm^{-1} (slopes b and c as seen on the green spectrum in Figure 3). The difference between the ash and dust signatures is that for the ash spectrum there is a visible change of slope gradient around 1160 cm^{-1}. As for the spectral signatures for water and ice clouds the monotonicity was opposite (positive) for the slope a (because of the reverse absorption behaviour for hydrous particles than ash particles) and slopes b and c were either flat or slightly negative.

These observations were the main basis for the new algorithm which uses the linear fits in the three regions, as seen in Figure 3. All the spectra were previously modified in such a way that the wavenumbers where water vapour optical depth was higher then 0.9 were removed from the spectra, to make the linear approximation work more efficiently (the red spectra in Figure 3). Figure 4 shows the three gradients calculated for every pixel over the Icelandic eruption on 7 May 2010. The ash cloud can be seen in blue and purple in the left picture, in red in the centre and in yellow and red in the right picture.

A new method for ash detection is proposed as follows:

1. For every pixel of the image determine the gradients of the three slopes for brightness temperature function between 842-965 cm^{-1} (gradient a), 1070-1160 cm^{-1} (gradient b) and 1160-1210 cm^{-1} (gradient c). Also calculate the absolute brightness temperature of the 3.7 µm channel averaged between 2670 and 2730 cm^{-1}.

2. Calculate the three ratios of the slopes in

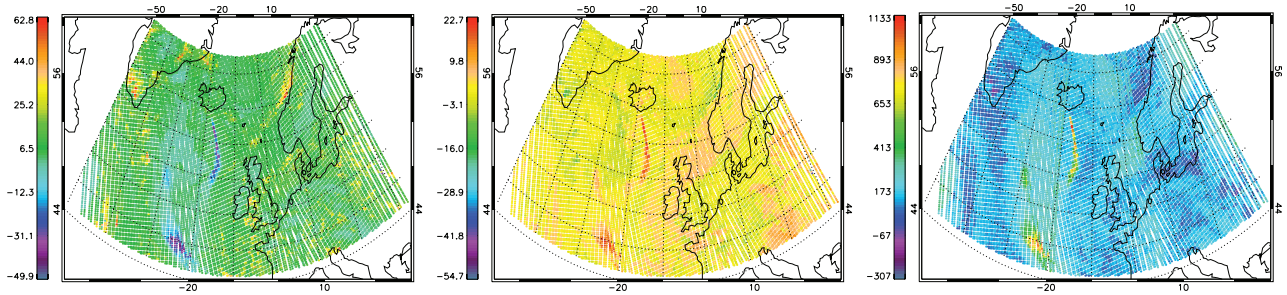

(a) Gradient a for wavenumbers between 842 and 965 cm^{-1}

(b) Gradient b for wavenumbers between 1070 and 1160 cm^{-1}

(c) Gradient c for wavenumbers between 1160 and 1210 cm^{-1}

Figure 4: The linear approximations for every pixel for the three regions of spectra as specified above for Eyjafjallajökull volcano eruption on Iceland, 7 May 2010. The gradients were multiplied by a factor of 10000 for convenience.

the following way:

$$r_1 = \frac{b}{a}, \quad r_2 = \frac{c}{b}, \quad r_3 = \frac{c}{a}$$

3. Two tests should now be carried out. All the following conditions must be met in each test to assume that a pixel is dominated by ash:

   (a) Test A (for pixels where no or little amounts of SO_2 are present):

   $$r_1 \leq -0.1,\ r_2 \geq 1.3,\ r_3 \in [-10, -0.2]$$

   $$a \leq 0, \quad b > 0, \quad c > 0.04$$

   $$BT_{3.7} \in [260, 305]$$

   (b) Test B (for pixels where vast amounts of SO_2 are present):

   $$r_1 \geq 0.1,\ r_2 \leq -2.6,\ r_3 \in [-20, -0.2]$$

   $$a \leq 0, \quad b < 0, \quad c > 0.04$$

   $$BT_{3.7} \in [260, 313]$$

4. Allocate all the pixels which are in 5 degrees latitude and longitude neighbourhood to the pixels which were found above to set the geographic region where the ash may occur.

5. The final condition for the ash flag is to correlate each of the local spectra (found in Test A or Test B) with each spectrum in a set of reference spectra which include 33% of the same local spectra (found in Test A or Test B) and 67% of spectral curves from different eruptions around the world since 2008 (the spectra from different eruptions were found and prepared earlier using Test A or Test B). The mean of all these correlation coefficients is then used as a threshold which is the cutting point for the ash flag.

As can be seen in point 3 of the ash test, there is a differentiation for eruption with large SO_2 spectral signatures (Test B) and without such signatures (Test A). This is because the shape of the ash spectrum which interferes with SO_2 has a negative slope in the second region, as can be

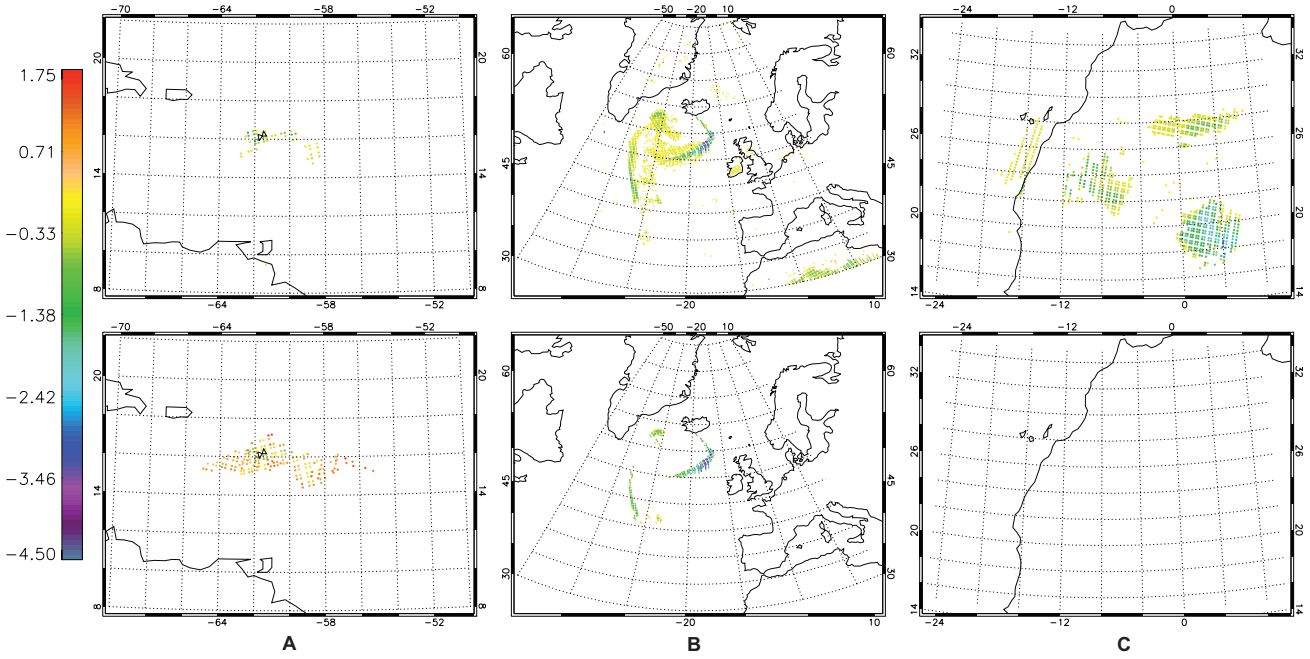

Figure 5: Brightness temperature difference for three case studies split in columns: A - the eruption of Montserrat volcano in the Caribbean Sea on 12 February 2010 at 13:50 UTC; B - the eruption of Eyjafjallajökull on 8 May 2010 at 21:14 UTC; C - the sand storm event on Saharan desert on 28 April 2010 at 12:59 UTC. The top three maps show the ash affected pixels according to the 'split-window' test (BTD is lower or equal to 0) and the bottom maps show the proposed method.

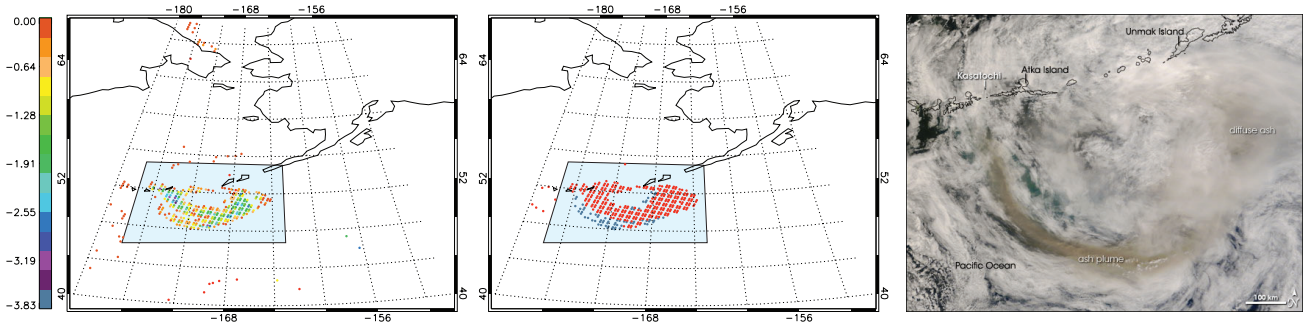

Figure 6: The left picture shows the result from the 'split-window' test from the Kasatochi eruption on 8 August 2008 at 21:15 UTC. The centre picture shows the same scene but using the new method (the red pixels are the pixels found from the Test B, while the blue colour marks the pixels found from the Test A). The area shaded in light blue is shown in the right picture in visible light using MODIS data acquired at 23:05 UTC (NASA Natural Hazards).

seen in Figure 3. Hence, to detect ash from this kind of event the modification to the test must be done.
Point 4 in the above technique is not necessary but improves the speed of the algorithm if large amounts of data are used.

2.2 Results

Figure 5 compares the 'split-window' test (11 and 12 µm channels centred at 924 and 835 cm^{-1}) with the proposed method. In the first column one can see the eruption from the volcano on Montserrat on 12 February 2010. This was the first day of the eruption and the proposed method detected a much larger area of ash plume then the 'split window' test. The plume flagged with the new method is continuous and finds many pixels where BTD is positive (up to +1.75). The correlation of the region to the right of the ozone band (1070-1210 cm^{-1}) may have given such results. There was only one false detection in BTD method over land which was not found by the new method.
In the second column the maps show the area on 8 May 2010 over the Atlantic Ocean, Europe and North Africa after the Eyjafjallajökull eruption. The ash cloud flagged using the proposed algorithm is more distinct and in the 'split-window' test many non ash pixels are detected including the desert dust pixels of the Sahara, while in the bottom picture no desert dust pixels were flagged; this is a very encouraging result as the previous methods, based on BTD, mistakenly detected desert dust pixels as ash pixels. This is because the desert dust and ash spectra have a very similar 'V' shaped curve.
The pictures in the next column show even better the important feature of this technique using the desert dust storm event for the Sahara on 28 April 2010. The 'split-window' test detected desert dust pixels both over the ocean and over the ground, while the new method does not detect any of them.
In the Kasatochi eruption in Alaska on 8 August 2008 vast amounts of SO_2 were emitted. In some areas the SO_2 was so dense that it severely changed the ash spectral curves in region 1070 - 1180 cm^{-1}, as can be seen in Figure 3. In this interesting eruption we could check the working features of the two tests described in point 3, chapter 2.1. The pixels found with Test A are marked with blue in Figure 6, while the red shows the area found by Test B. Using only one of these tests would not find the ash plume properly as the SO_2 is concentrated in the centre of the plume, and there is some ash, mainly in the vicinity of the plume, where smaller amounts of SO_2 are present. This is a good result because in eruptions like this one SO_2 does not always follow the ash plume and by this method both kinds of plumes can be detected. In this example it is also seen that this method works well even in the areas where large amounts of water clouds are present.
Similar behaviour is seen in the Sarychev Peak

eruption in June 2009.

3 Characteristic properties of ash

3.1 Method

In the 2010 Eyjafjallajökull eruption the ash was mainly composed of andesite (Ilyinskaya et al., 2011) which has a lower concentration of SiO_2 than the rhyolite which was the main constitution of the 2008 Chaiten eruption (Carn et al., 2009). As can be seen in Figure 2, the spectrum for rhyolite ash has a quadratic shape in the region 800-960 cm^{-1} while the andesite ash has a rather linear or a very wide quadratic dependence on wavenumber (Gangale et al., 2009). These properties were used to determine if a particular ash spectrum had rhyolitic or andesictic composition. Two hundred ash spectra were analyzed to find the threshold for the concavity. The test is proposed as follows:

- If the concavity in the 800-925 cm^{-1} region is lower then -0.0009 and the maximum of parabola lies between 800 and 900 cm^{-1} the ash is **rhyolitic**.
- If however the concavity in the same region is larger then -0.0009 the ash is **andesitic**.

3.2 Results

Figure 7 shows the eruption from the Chaiten volcano in Chile on 5 May 2008 (the eruption started on 2 May 2008). The test for the concavity does not straightforwardly confirm that the ash from this eruption is rhyolitic, because only 43% of all pixels flagged as ash had concavity lower then -0.0009, marking it as rhyolite. The result from the 'split-window' test can be seen in Figure 7 i. A lot of pixels over area B (as seen in the picture) are not flagged as ash by this method and the proposed algorithm marks more pixels as ash making the plume more continuous (Figure 7 ii). Moreover the pixels flagged with the new method over area B have positive BTD (as in the Montserrat eruption, Figure 5 A). The eruption lasted for three days and ash over area A may have laid down on the ground, while ash over area B may be mostly in the air. The picture from this area on that day can be also seen in the visible spectrum in Figure 12 in Appendix A.

An interesting thing happens when we add another restriction given by Gangale et al. (2009), which is that the spectrum of ash pixels must have a negative concavity in the region 800-960 cm^{-1}. The pixels in area A are mostly neglected, as can be seen in Figure 7 iii. When the same condition for concavity is checked on a smaller region (800-925 cm^{-1}) not as many pixels are neglected as in the 800-960 cm^{-1} range. This may mean that ash in area A might have changed its composition a little.

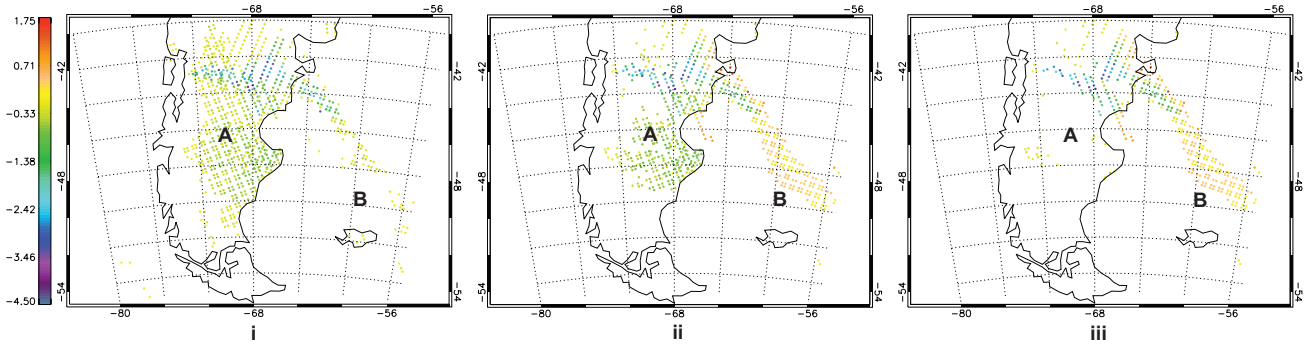

Figure 7: Eruption from the Chaiten volcano in Chile, 5 May 2008, 13:56 UTC. i - 'split-window' test where BTD < 0; ii - the result from the proposed method; iii - as in ii) but pixels where the concavity in region 800-960 cm^{-1} is greater then 0 are neglected.

4 A fast retrieval of ash plume properties

4.1 Method

To find the characteristic properties of the plume, simulations of the ash spectra must be used as generated by radiative transfer code (ORAC). The simulation spectra were a function of the optical depth, height and effective radius of ash particles for particular optical properties of given tephra (e.g. andesite). These three variables were changed in order to fit the IASI real spectra as follows.

1. The first property to be found was the optical depth of the plume which ranged from 0.2 to 2 with an interval of 0.2. For each value of optical depth the height was varied from 0 to 10 km in an interval of 0.5 km above the surface, and consecutively the effective radius was varied from 0.8 to 2 µm in an interval of 0.1µm. Every pixel was than correlated with this set of simulation curves. The best value of optical depth for a given pixel was established when the mean of a set of correlation coefficients for the set of heights and effective radii was maximum.

2. With fixed optical depth (found above) for a given pixel, the height was then found by varying the effective radius in the same manner as before. The height was again established for the largest mean of correlation coefficients.

3. For every pixel of the ash plume the optical depth and cloud-top-height was fixed. The effective radius was varied again and the value of the effective radius for a given pixel was established for the maximum correlation coefficient between the simulation and real spectra.

The means were taken rather than the maximum of the correlation because it was possible that the maximum would occur for some random combination of optical depth, height and effective radius, while the mean would give a good picture of the variation of a given variable; choose the maximum from this set to find the best value of a variable.

4.2 Results

Using simulations of ash spectra generated by ORAC some properties of ash plumes can be extracted from IASI data if appropriate refractive index properties of ash are used. Figure 8 depicts spectral shapes for three values of effective radius 0.9, 1.2, 1.5 μm and fixed cloud top height and optical depth. From these simulations it is clearly seen that the larger the effective radius the larger are all the slopes and BTD. Similarly, this applies to optical depth and cloud top height. The denser and higher the plume in the atmosphere the larger the gradients of the spectra. As can be seen in Figure 8, the real spectra in region 800 - 980 cm^{-1} fit quite well the green curve, while in the region 1070-1200 cm^{-1} the red curve fits better. Hence the trick of the algorithm was to find the best correlation of these curves.
These simulations were used to estimate the properties from the Eyjafjallajökull ash plume over the Atlantic Ocean on 7 May 2010. According to Gasteiger et al. (2010) the ash from this eruption is mainly andesitic, which was also

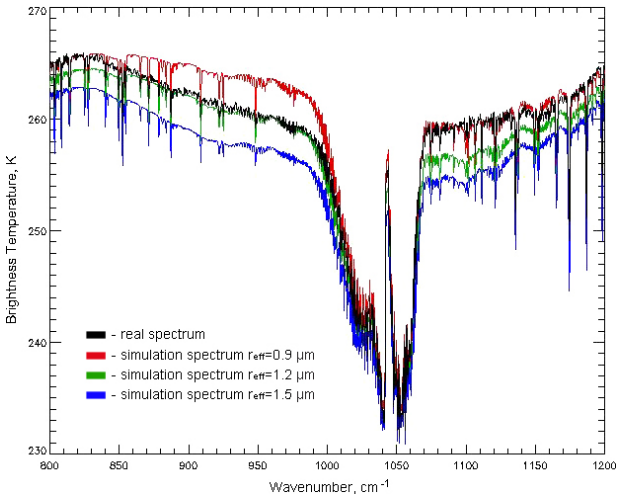

Figure 8: Ash spectral curves. The black line shows one IASI spectrum from the Eyjafjallajökull eruption on 7 May 2010; red, green and blue are simulations of spectra with optical depth = 0.8 and CTH = 3 km and the effective radius is changed as seen in the picture.

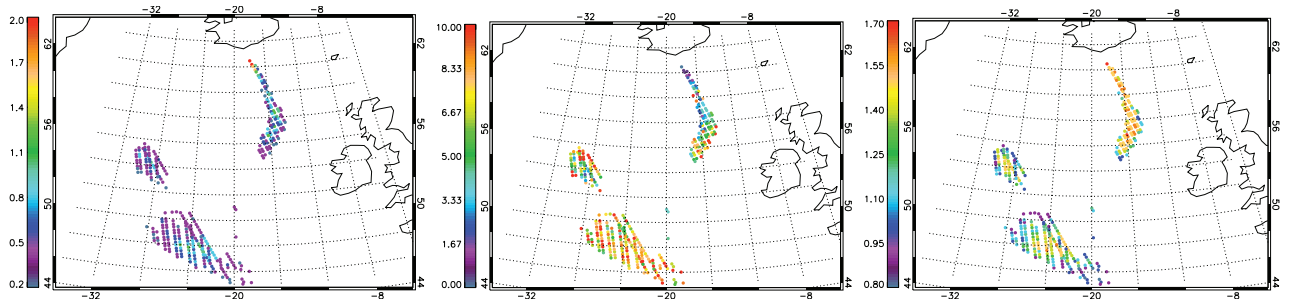

(a) Optical depth, 1 **(b)** Cloud top height, km **(c)** Effective radius, μm

Figure 9: The figures show the characteristic properties of ash plumes for the Eyjafjallajökull eruption on 7 May 2010. The picture on the left shows optical depth of the plume, the second shows the cloud top height and the third the effective radius of the ash particles.

confirmed by the test from point 2.2 as 67% pixels appeared to satisfy the conditions for the andesitic ash. The results for the retrieval of plume properties are quite encouraging, as the optical depth (Figure 9a) is highest where the plume is the freshest and it is decreasing further away from the volcano. The centres of each of the three 'ash plume islands' are the mostly dense as they are less dispersed by the wind and the optical depth is also higher. The cloud top height is the smallest where the ash cloud is youngest; however it should not be equal to zero. The other CTH are in reasonable range. One can suppose that the effective radius is also highest in the fresh plume because the bigger particles did not have enough time to fall down under the reaction of gravity, which is what happens on later occasions. In the older plumes the radius is also changing but the mean for each of the two islands is about 1.3. According to Gasteiger et al. (2010) the mean effective radius of ash particles over München on 28 of April was 1.55 µm. The simulation was also done for the Chaiten and Kasatochi eruptions using the andesitic refractive index properties, but the results were not as good as for the Icelandic eruption.

5 Flag accuracy and efficiency

To find the efficiency of the proposed algorithm two tests were done over a very large area on random days where no ash should be present. The proposed algorithm was run over the Pacific on 17 April 2008 and has not detected any ash pixels, while the 'split-window' test detected ash as 1.24% of all the pixels over this area. Similar results were obtained on 21 January 2009 over the same area. BTD was negative for 3.4‰ of all pixels when the proposed method has not detected any.

The First map in Figure 10 shows the correlation coefficients for all the pixels after the eruption of Eyjafjallajökull. These coefficients may now be used as a kind of certainty that a given pixels is ash affected or not. The ash plume is clearly marked with red and the coefficients range between around 0.9 and 0.7. No other areas are marked with red as clearly as the ash plume. The desert dust detected by the 'split-window' test (as seen in Figure 5) is marked with yellow and the coefficient is around 0.5.

In the second map the same coefficient was calculated for the retrieval of the plume properties. The picture shows the coefficients for the cloud top height retrieval. Pixels in the middle of each volcanic plume island are correlated the best.

The last picture shows the quadratic fits in the spectral region 800 - 960 cm^{-1}. The fit for volcanic ash pixels is clearly negative while the quadratic coefficients for water clouds and clear scene spectra are positive or nearly zero (compare with Figure 12 in Appendix A).

6 Conclusions

6.1 Summary

Developing a precise algorithm to find the ash in the atmosphere is a difficult and complex task, as

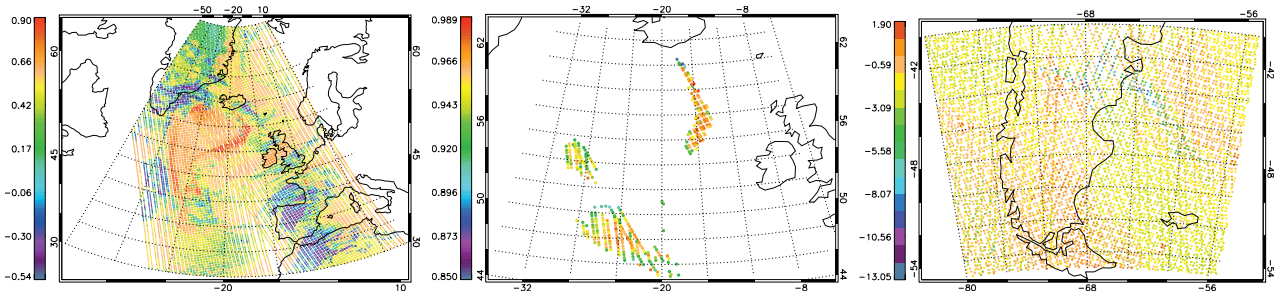

(a) Ash detection from Eyjafjallajökull erruption, 8 May 2010

(b) Height correlation on Eyjafjallajökull eruption, 7 May 2010

(c) Quadratic fits on Chaiten eruption, 5 May 2008

Figure 10: The first two maps show the correlation coefficients for the results explained above. The picture on the right shows the quadratic fit for all pixels (the coefficients were multiplied by a factor of 10000 for convenience).

the composition of volcanic plumes varies significantly from one eruption to another. The 'split-window' test has been used to satisfying results for over 20 years. However, with the introduction of high resolution infrared spectrometers new algorithms could be produced. The method presented above, using the ratios of the three slopes of the spectra and correlation coefficients, has never been used before as IASI was introduced quite recently, in 2006. It is working well in most of the eruptions that have been investigated, although in different climates or atmospheric conditions small adjustments to the threshold may be required for it to be more precise. The threshold established by the correlation may not be very exact at all times but there is a clear distinction between ash and other aerosols. An example of this is the threshold set on data from 17 April 2010 after the Eyjafjallajökull eruption which found ash only over the Atlantic, but when we look at Figure 11a the ash is clearly visible over Europe, England and also over the Atlantic Ocean close to France; this is not distinctly visible in the 'split-window' test as seen in Figure 11b and c. This algorithm is not computionally exhausting and can be used in real time situations to localize the ash clouds.

6.2 Further work

A few improvements to this method could be introduced in the future. The test for the concavity could be conducted before the test with slopes and ratios to give an idea of whether the ash is rhyolitic or andesitic, and then special conditions for different compositions could be applied. It is proposed to set up a large database with refractive indexes from different eruptions all over the world so that the retrieval of plume properties using simulation curves can be done more efficiently.

Acknowledgements
The author would especially like to thank Dr. E.

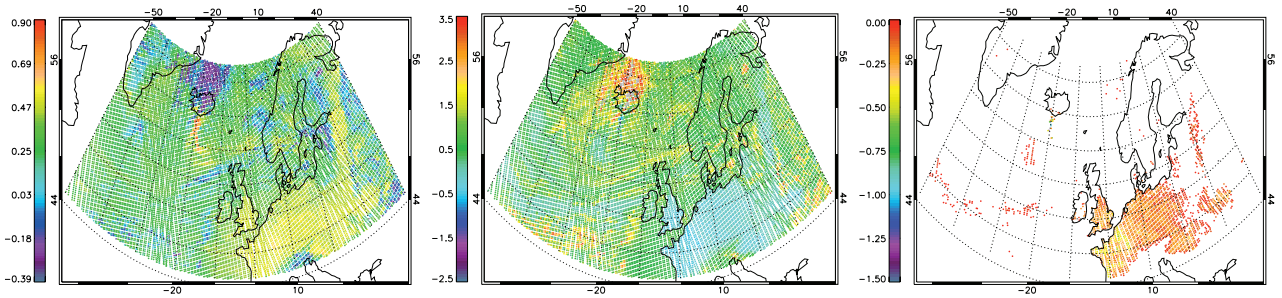

(a) Correlation coefficient

(b) Brightness temperature difference

(c) Brightness temperature difference lower or equal to 0

Figure 11: Eyjafjallajökull eruption on 17 April 2010.

Carboni, Dr. R.G. Grainger and Dr. G. Thomas for the substantial help, provision of the IASI data and all the support they gave me in this project.

References

[1] Beer, R., Norton R., Analysis of spectra using correlation functions. *Applied Optics*, 27:1255-1261, 1987.

[2] Carn S. A., Pallister J. S., Lara L., Ewert J. W., Watt S., Prata A. J., Thomas R., Villarosa G. The re-awakening of Chaitn volcano. *EOS*, 90(24), 205-207, 2009.

[3] Casadevall T.J. The 1989/1990 eruption of Redoubt Volcano Alaska: impacts on aircraft operations. *Journal of Volcanology and Geothermal Research*, 62: 301316, 1994.

[4] Clarisse L., Prata A.J., Lacour J.L., Hurtmans D., Clerbaux C., Coheur P.F., A correlation method for volcanic ash detection using hyperspectral infrared measurements. *Geophysical research letters*, 37, L19806, doi:10.1029/2010GL044828, 2010.

[5] Colette A., Favez O., Meleux F., Chiappini L., Haeffelin M., Morille Y., Malherbe L., Papin A., Bessagnet B., Menut L., Leoz E., Roul L., Assessing in near real time the impact of the April 2010 Eyjafjallajkull ash plume on air quality. *Atmospheric Environment*, 45, 1217-1221, doi:10.1016/j.atmosenv.2010.09.064, 2010.

[6] Ellrod G.P., Connell B. H., Hillger D. W., Improved detection of airborne volcanic ash using multispectral infrared satellite data. *Journal of Geophysical Research*, 108(D12):4356. doi:10.1029/2002JD002802, 2003.

[7] Gangale G., Prata A.J., Clarisse L., The infrared spectral signature of volcanic ash determined from high-spectral resolution satellite measurements. *Remote Sens. Environ.*, 114, 414-425, doi:10.1016/j.rse.2009.09.2007, 2009.

[8] Gasteiger J., Groß S., Freudenthaler V., Wiegner M, Volcanic ash from Iceland over Munich: mass concentration retrieved fromground-based remote sensing measurements. *Atmospheric Chemistry and Physics Discussions*, 10, 2670526750, doi:10.5194/acpd-10-26705-2010, 2010.

[9] Hillger D. W., Clark J.D., Principal component image analysis of MODIS for volcanic ash. Part I: most important bands and implications for future GOES imagers. *Journal of Applied Meteorology*, 41:9851001, 2002.

[10] Hillger D.W., Clark J.D., Principal component image analysis of MODIS for volcanic ash. Part II: simulation of current GOES and GOES-M imagers. *Journal of Applied Meteorology*, 41:10031010, 2002.

[11] Holasek R.E., Rose W.I., Anatomy of 1986 Augustine volcano eruptions as recorded by multispectral image processing of digital AVHRR weather satellite data. *Bulletin of Volcanology*, 53:420-435, 1991.

[12] Ilyinskaya E., Tsanev V.I, Martin R.S., Oppenheimer C., Le Blond J., Sawyer G.M., Gudmundsson M.T., Near-source observations of aerosol size distributions in the eruptive plumes from Eyjafjallajkull volcano, MarchApril 2010. *Atmospheric Environment*, doi: 10.1016/j.atmosenv.2011.03.017, 2011.

[13] Karagulian F., Clarisse L., Clerbaux C., Prata A.J., Hurtmans D., Coheur P.F, Detection of volcanic SO2, ash, and H2SO4 using the Infrared Atmospheric Sounding Interferometer (IASI). *Journal of Geophysical Research*, 115, doi:10.1029/2009JD012786, 2010.

[14] Mastin L.G., Guffanti M., Servranck R., Webley P., Barsotti S., Dean K., Durant A.,Ewert J.W., Neri A., Rose W.I., Schneider D., Siebert L., Stunder B., Swanson G., Tupper A., Volentik A., Waythomas C.F., A multidisciplinary effort to assign realistic source parameters to models of

volcanic ash-cloud transport and dispersion during eruptions. *Journal of Volcanology and Geothermal Research*, 186, 10-21, doi:10.1016/j.jvolgeores.2009.01.008, 2009.

[15] Miller T.P., Casadevall T.J., Volcanic ash hazards to aviation. *Encyclopedia of Volcanoes. Academic Press.*, 915930, 2000.

[16] Mosher F.R., Four channel volcanic ash detection algorithm. *Preprint Volume*, 457-460, 2000.

[17] Pavalonis M.J. , Feltz W.F., Heidinger A.K., Gallina G.M., A Daytime Complement to the Reverse Absorption Technique for Improved Automated Detection of Volcanic Ash. *Journal of Atmospheric and Oceanic Technology*, 23, 1422-1444, 2006.

[18] Pergola N., Tramutoli V., Marchese F., Scaffidi I., Lacav T., Improving volcanic ash cloud detection by a robust satellite technique. *Remote Sensing of Environment*, 90:122, 2004.

[19] Prata A.J., Observations of volcanic ash clouds in the 10-12μm window using AVHRR/2 data. *International Journal of Remote Sensing*, 10(4-5):751761, 1989a.

[20] Prata A.J., Infrared radiative transfer calculations for volcanic ash clouds. *Geophysical Research Letters*, 16(11):1293-1296, 1989b.

[21] Prata A.J., Bluth G., Rose B., Schneider D., Tupper A., Comments on Failures in detecting volcanic ash from a satellite-based technique. *Remote Sensing of Environment*, 78, 341-346 2001.

[22] Prata A.J., Grant I.F., Retrieval of microphysical and morphological properties of volcanic ash plumes from satellite data: Application to Mt Ruapehu, New Zealand. *Q. J. Royal Meteorological Society*, 127, 2153-2179 2001.

[23] Prata A.J., Satellite detection of hazardous volcanic clouds and the risk to global air traffic. *Natural Hazards*, 51, 303-324, doi:10.1007/s11069-008-9273-z 2008.

[24] Simpson J.J., Hufford G., Pieri D., Berg J., Failures in detecting volcanic ash from a satellite-based technique. *Remote Sensing of Environment*, 72:191217 2000.

[25] Sturkell E., Einarsson P., Sigmundsson F., Geirsson H., O lafsson H., Pedersen R., de Zeeuw-van Dalfsen E., Linde A.T., Sacks S.I., Stefansson R., Volcano geodesy and magma dynamics in Iceland. *Journal of Volcanology and Geothermal Research*, 150, 14-34, doi:10.1016/j.jvolgeores.2005.07.010 2006.

[26] Thomas G.E., Carboni E., Sayer A.M., Poulsen C.A., Siddans R., Grainger R.G. Oxford-RAL aerosol and cloud (ORAC): Aerosol retrievals from satellite radiometers. *Aerosol Remote Sensing Over Land, Springer*, 2009.

[27] Textor C., Graf H.F., Herzog M., Oberhuber J.M., Rose W.I., Ernst G.G.J., Volcanic particle aggregation in explosive eruptive columns. Part I: Parameterization of the microphysics of hydrometeors and ash. *Journal of Volcanology and Geothermal Research*, 150, 359-377 2005.

[28] Textor C., Graf H.F., Herzog M., Oberhuber J.M., Rose W.I., Ernst G.G.J., Volcanic particle aggregation in explosive eruptive columns. Part II: Numerical experiments. *Journal of Volcanology and Geothermal Research*, 150, 378-394 2005.

[29] Wearden G., Ash cloud costing airlines 130m a day. *The Guardian*, 2010.

[30] Wiegner M., Gasteiger J., Groß S., Schnell F., Freudenthaler V., Forkel R., Characterization of the Eyjafjallajkull ashplume: Potential of lidar remote sensing. *Physics and Chemistry of the Earth*, doi:10.1016/j.pce.2011.01.006 2011.

[31] Yu T., Rose W.I., Prata A.J., Atmospheric correction for satellite-based volcanic ash mapping and retrievals using split window IR data from GOES and AVHRR. *Journal of Geophysical Research*, 107, doi:10.1029/2001JD000706 2002.

A Appendix

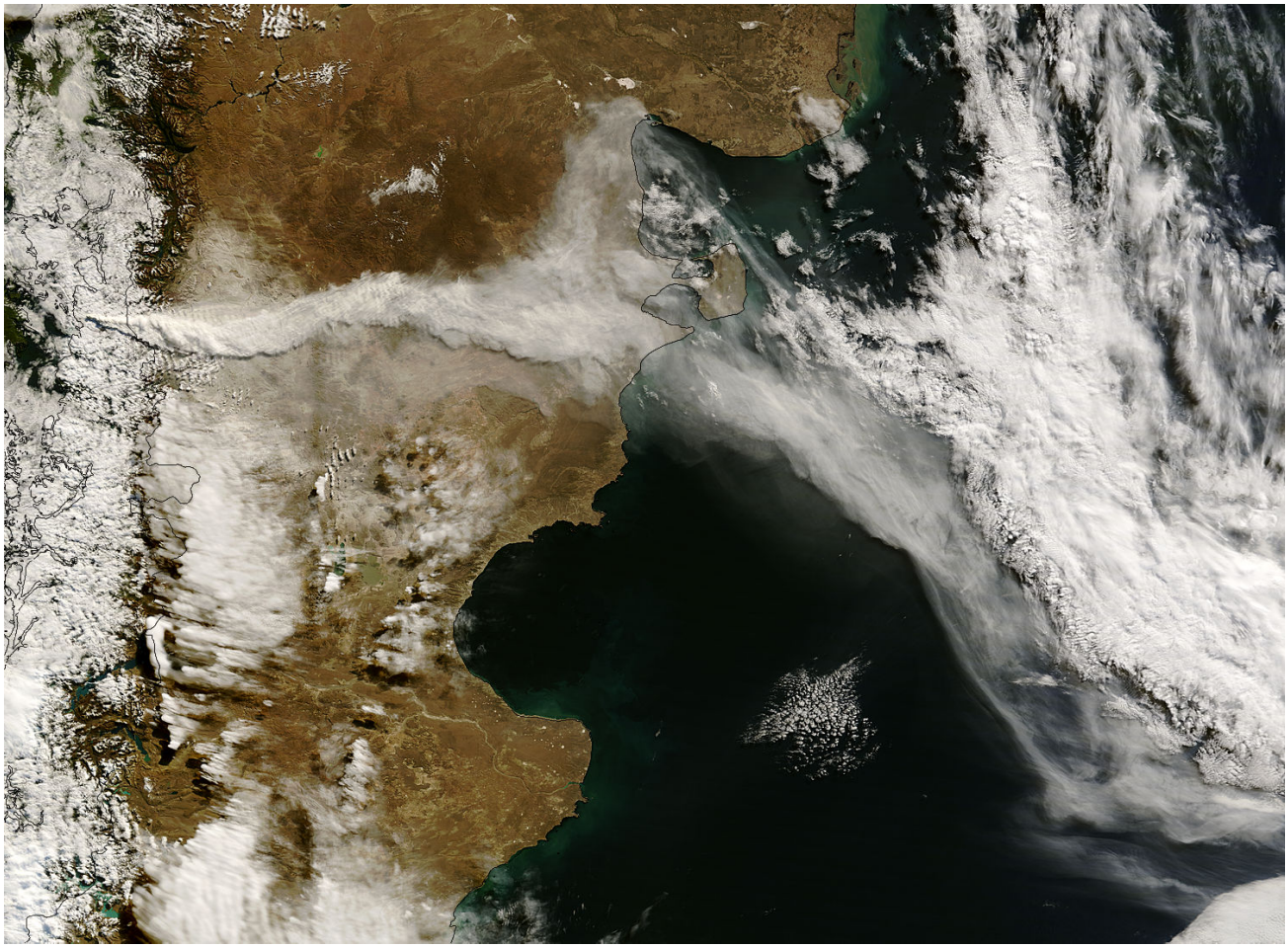

Figure 12: Picture from MODIS in visible light, South America, 5 May 2008.